Broadband Statistically Designed Thinned-Binned Array Antennas

Giovanni Buonanno, *Member, IEEE*, Sandra Costanzo, *Senior Member, IEEE*, and Raffaele Solimene, *Senior Member, IEEE*

***Abstract*— Statistically thinned arrays are obtained by thinning a reference filled array, according to a probabilistic law that is dictated by the reference current. The remaining radiators are still separated by commensurable distances, even if randomly located. Hence, wideband operations are prevented by grating lobes' occurrence. To overcome the above limitation, a new and simple strategy is presented in this article for randomly deploying the elemental radiators across the array aperture. More in detail, unlike classic thinned arrays, elements surviving the thinning are not positioned on a priori fixed deterministic lattice. Instead, their positions are modeled as random variables, which are determined by exploiting the binned strategy. Numerical examples reveal that the new proposed scheme allows for a considerable enlargement of the frequency band, without incurring in grating lobes' appearance.**

***Index Terms*— Density-tapered arrays, nonuniformly spaced arrays, random binned arrays, thinned arrays.**

NOMENCLATURE

$\phi(u,v)$	Reference array factor.
$i(x,y)$	Reference aperture current.
$F_k(u,v)$	Array factor ($k=1$ for statistically thinned arrays and $k=2$ for statistically thinned-binned arrays).
$\overline{F_k(u,v)}$	Mean of the array factor ($k=1$ for statistically thinned arrays and $k=2$ for statistically thinned-binned arrays).
$\sigma_k^2(u,v)$	Variance of the array factor ($k=1$ for statistically thinned arrays and $k=2$ for statistically thinned-binned arrays).
$MSE_k(u,v)$	Mean square error between the actual and reference array factors ($k=1$ for statistically thinned arrays and $k=2$ for statistically thinned-binned arrays).
$P_k(u,v)$	Power pattern ($k=1$ for statistically thinned arrays and $k=2$ for statistically thinned-binned arrays).
$\overline{P_k(u,v)}$	Mean of the power pattern.
$\sigma_P^2(u,v)$	Variance of the power pattern (subscript k is omitted for simplicity).
$F_{\mathcal{R}}(u,v)$	Real part of the array factor (subscript k is omitted for simplicity).
$F_{\mathcal{I}}(u,v)$	Imaginary part of the array factor (subscript k is omitted for simplicity).
$\mu_{\mathcal{R}}(u,v)$	Mean of $F_{\mathcal{R}}(u,v)$.
$\mu_{\mathcal{I}}(u,v)$	Mean of $F_{\mathcal{I}}(u,v)$.
$\sigma_{\mathcal{R}}^2(u,v)$	Variance of $F_{\mathcal{R}}(u,v)$.
$\sigma_{\mathcal{I}}^2(u,v)$	Variance of $F_{\mathcal{I}}(u,v)$.
$\mathcal{K}(u,v)$	Covariance function of $F_{\mathcal{R}}(u,v)$ and $F_{\mathcal{I}}(u,v)$.
$\mathcal{LS}_\eta^2(u,v)$	η-percent level surface.

Manuscript received 6 August 2022; revised 3 December 2022; accepted 13 December 2022. Date of publication 19 January 2023; date of current version 6 March 2023. *(Corresponding author: Giovanni Buonanno.)*

Giovanni Buonanno and Sandra Costanzo are with the Dipartimento di Ingegneria Informatica, Modellistica, Elettronica e Sistemistica (DIMES), Università della Calabria, 87036 Rende, Italy (e-mail: giovanni.buonanno@unical.it; costanzo@dimes.unical.it).

Raffaele Solimene is with the Dipartimento di Ingegneria, Università della Campania, 81031 Aversa, Italy (e-mail: raffaele.solimene@unicampania.it).

Color versions of one or more figures in this article are available at https://doi.org/10.1109/TAP.2023.3236793.

Digital Object Identifier 10.1109/TAP.2023.3236793

I. INTRODUCTION

WHEN a very narrow beam is required to comply with high resolution, large antenna arrays should be used. If a uniform space between the radiators is chosen, a huge number of elements must be distributed over the array aperture. Indeed, since the main-beam width is mainly linked to the size of the array aperture, whereas the number of radiators basically impacts the sidelobe structure, the number of radiators can be greatly reduced [1], [2], [3], [4].

To this end, thinned arrays are one of the most efficient and widely adopted option allowing to reduce the system weight and simplifying the feeding network. Indeed, since isophoric excitation coefficients are generally adopted, amplifiers can operate at the peak efficiency [5]. For these reasons, thinned arrays can be positively exploited in various scenarios, such as satellite communications, radio astronomy, high-resolution ground-based radars, adaptive arrays, as well as in all those applications where resolution matters more than gain [6], [7], [8].

Thinned arrays are obtained by removing/turning off some elements from a preassigned array grid [9]. Typically, the starting grid is a periodic one. To achieve such a task, different methods have been proposed in the literature.

Many methods cast the problem in terms of a constrained optimization. In this framework, many randomized search algorithms have been proposed and compared in the literature [10], [11], [12], [13], [14], [15]. These methods offer a certain degree of flexibility since constraints for beam pattern shaping can be embodied in the optimizations stage. However,

they require to heuristically set a number of parameters, and what is more, the high computational cost makes them better suited for small- and medium-sized arrays [9].

The iterative Fourier technique introduced in [16], and its developed versions [17], [18], exploits the Fourier transform relationship between the excitation coefficients and the pattern. This technique can require a lower computational cost, thus being usefully adopted for large arrays, in principle; however, it still requires running an iterative algorithm and the choice (heuristic) of a threshold for declaring which element must be turned on. Therefore, like the other techniques mentioned above, even this methodology does not allow to provide an a priori analytic description of the performance.

Let us also mention the dynamic programming approach presented in [19]. This method is deterministic and applicable to large arrays. Numerical results reported in [19] prove the effectiveness of this technique, although based on a suboptimal optimization procedure.

Thinned arrays can be designed using a statistical approach as well [5]. Indeed, in the so-called statistically designed density-tapered arrays [5], also addressed as statistically thinned arrays (STAs) [20], one starts from the reference filled array (generally a half wavelength spaced array) and then removes radiators by tossing a coin. In particular, the excitation coefficients are modeled as binary Bernoulli random variables that are used to determine whether an element is switched ON or OFF [9]. Moreover, since the Bernoulli variable distributions are linked to the excitation coefficients of the reference array factor, spatial-density tapering is obtained. Compared to the previously mentioned thinning methods, STAs are extremely quick. For this reason, they are suited for large and very large arrays, and they have also been suggested for real-time adaptive pattern formation [7]. On the contrary, only the average array factor is guaranteed to be equal to the reference array factor. Instead, the array factor is a random process statistically oscillating around the average one. Therefore, to accurately predict the key radiation pattern parameters (such as the peak sidelobe level), the statistical characterization of such a random process is required. Usually, the second-order moment, i.e., the average power pattern, is considered. However, this is not enough to foresee the statistical fluctuations of the pattern. Recently, a rigorous and complete statistical description of STAs has been provided in [21]. Also, STAs are usually employed for single-beam patterns, whereas in [22], it is shown that STAs can be employed to generate multibeam patterns.

The starting array grid is usually uniform. Hence, after the thinning, the distances between the remaining radiators are commensurable, and thus, grating lobes occur when the operation frequency increases. Indeed, STAs are actually random periodic arrays [24].

In order to achieve a broadband behavior, in this article, we propose a new and simple strategy that merges the classical STAs with the so-called binned arrays [25]. More in detail, after the statistical thinning, the position of each element that remained in the grid is randomly moved within a bin centered around the initial element's location. The proposed method preserves the very low computational cost, and it inherits the STAs's ability to reduce the number of elements, as well as the very large bandwidth (without grating lobes) instead characterizing the binned arrays. In addition, unlike totally random arrays [1], [26], [27], the binning step also imposes some constraints on the radiators' positions so that only the adjacent ones could be closed. More in detail, due to the binned step, each radiator is deployed according to a uniform probability density function only within a single bin. This entails that the array aperture is (probabilistically) more "uniformly" filled with respect to the space tapering [28] and to the totally random arrays. As a further aspect, mutual coupling can be considered less relevant. Moreover, it is worth highlighting that the proposed methodology is so flexible that it can be applied advantageously also in reflectarrays applications [29], [30] and, due to the characteristics of the treated arrays, it can exploit broadband matching techniques [31] and wideband methodologies for the integration of different technologies [32].

The array factor provided by the new proposed scheme is of course still a random process. Therefore, also, in this case, the estimation of the statistical features of the array factor must be pursued, and this is actually the main contribution to be pursued in this article. To this end, the mean square error (MSE) between the random array factor and the reference one is first derived. This is related to the mean power pattern that, in the sidelobe region, is commonly employed to estimate the sidelobe level. However, we go a bit further. We derive also the power pattern variance that, due to Cantelli's inequality, allows to obtain an easy way to compute a lower bound for the cumulative distribution function of the power pattern. Then, this result is refined by assuming a certain symmetry for the reference current. These theoretical results allow for a more accurate characterization of the power pattern statistical fluctuations and allow to introduce isosurfaces below which the pattern resides with an assigned probability. In particular, since the isosurfaces are analytically linked to the parameters of the array (i.e., the reference excitation currents, the number of elements in the original grid, and the thinning level), it is possible to a priori estimate the array factor features. Vice versa, such results allow for array synthesis since one can set the array characteristics, which ensures, with a given probability, the array factor properties.

Eventually, the new scholar content conveyed in this article concerns: the introduction (for the first time, at the authors' knowledge) of a combined thinned/binned scheme and a rigorous theoretical treatment allowing to estimate the array factor probability distribution, which in turn permits to foresee the array factor behavior and to link it to the array parameters. In particular, previous expertise developed while addressing separately thinned arrays [21], [22] and binned arrays [27], [33], [36] is applied, to the combined case at hand. Finally, as opposed to our previous contributions, 2-D arrays are addressed here.

This article also includes a numerical section and an appendix. The former is devoting to show some selected numerical experiments that highlight a considerable frequency band enlargement (compared to classic STAs). The Nomenclature consists of a glossary of the most important quantities, whereas

the Appendix details some mathematical derivations that are omitted in the main text.

II. Problem Statement

Let us consider a planar array whose aperture is defined as $[-L_x/2, L_x/2] \times [-L_y/2, L_y/2]$, with L_x and L_y being the array dimensions in meters. Let $u = \sin\theta\cos\phi - \sin\theta_0\cos\phi_0 \in [-2, 2]$ and $v = \sin\theta\sin\phi - \sin\theta_0\sin\phi_0 \in [-2, 2]$ be the observation variables, with $\theta \in [0, \pi]$ and $\phi \in [0, 2\pi]$ being the elevation and the azimuth angles, respectively, and (θ_0, ϕ_0) represents the steering direction. The circularly bounded domain, D, centered at the origin of the uv plane, and having radius equal to 2 represents the so-called full scan range [34].

We start by the following problem: given the space factor $\phi(u, v)$ due to a real and positive aperture current $i(x, y)$, i.e.,

$$\phi(u,v) = \int_{-L_x/2}^{L_x/2}\int_{-L_y/2}^{L_y/2} i(x,y) e^{j\frac{2\pi}{\lambda}(xu+yv)} dxdy \tag{1}$$

in which λ is the wavelength in vacuum and x and y are in meters, find an approximation of $\phi(u, v)$ in terms of the following array factor (the mutual coupling between radiators is assumed to be negligible [1], [3], [25], [26])

$$F(u,v) = C\sum_{n=1}^{N} B_n e^{j\frac{2\pi}{\lambda}(x_n u + y_n v)} \tag{2}$$

with B_n, x_n, and y_n being random variables.

It must be remarked that the usual framework for random arrays is to consider uniform excitation coefficients. This is because beam shaping can be achieved, to some extent, through the (random) space-density tapering. Actually, it has been shown that random excitation coefficients (which are dependent on the random positions) can allow for a more general shaping [27]. However, this type of random arrays is ruled out in the present study.

For thinning purposes, the coefficients B_n are relevant only to decide if elements should remain in the array. Hence, they are assumed to be Bernoulli random variables, that is, $P(B_n = 1) = p_n$ and $P(B_n = 0) = 1 - p_n$, with $0 \le p_n \le 1$. Since B_n, x_n, and y_n are random variables, $F(u, v)$ is a stochastic process. Accordingly, the corresponding synthesis problem is formulated in terms of their determination, by imposing that the average array factor matches the desired one, that is, $\overline{F(u,v)} = E[F(u,v)]$ be as close as possible to $\phi(u, v)$. To this end, in the following, we first briefly recall the basics concerning classic STAs. This is done to make this article self-contained, to introduce the necessary notation and to establish a reference against which to compare the new random scheme. Then, the new hybrid scheme is introduced.

III. Classic STAs

As mentioned above, STAs lead to random periodic arrays, which are obtained by removing radiators from a uniform-filled array, according to a probabilistic law. The resulting array factor can be written as [5]

$$F_1(u,v) = C_1\sum_{n=1}^{N_x}\sum_{m=1}^{N_y} F_{nm} e^{j\frac{2\pi}{\lambda}(x_{nd}u + y_{md}v)} \tag{3}$$

where $\{F_{nm}\}$ are Bernoulli random variables and

$$x_{nd} = -\frac{L_x}{2} + \frac{L_x}{2N_x} + (n-1)\frac{L_x}{N_x} \quad \text{for } n = 1, \ldots, N_x \tag{4}$$

$$y_{md} = -\frac{L_y}{2} + \frac{L_y}{2N_y} + (m-1)\frac{L_y}{N_y} \quad \text{for } m = 1, \ldots, N_y. \tag{5}$$

The corresponding average array factor is then given by

$$\overline{F_1(u,v)} = C_1\sum_{n=1}^{N_x}\sum_{m=1}^{N_y} p_{nm} e^{j\frac{2\pi}{\lambda}(x_{nd}u + y_{md}v)} \tag{6}$$

with $p_{mn} = \overline{F_{nm}}$.

In order to lead $\overline{F_1(u,v)}$ approximating $\phi(u, v)$, the terms p_{nm} must be necessarily related to $i(x, y)$. In particular,

$$p_{nm} = \alpha\frac{i(x_{nd}, y_{md})}{\max\{i(x_{nd}, y_{md})\}}. \tag{7}$$

The constant $0 < \alpha \le 1$ determines the intensity of the thinning. When $\alpha = 1$, the natural thinning is obtained. Thinning can be made more severe by reducing α. Now, if

$$C_1 = \frac{L_x L_y}{\alpha N}\max\{i(x_{nd}, y_{md})\} \tag{8}$$

with $N = N_x N_y$, then (6) is rewritten as

$$\overline{F_1(u,v)} = \frac{L_x L_y}{N}\sum_{n=1}^{N_x}\sum_{m=1}^{N_y} i(x_{nd}, y_{md}) e^{j\frac{2\pi}{\lambda}(x_{nd}u + y_{md}v)} \tag{9}$$

which clarifies how $\overline{F_1(u,v)}$ approximates $\phi(u, v)$. Indeed, (9) can be seen as a zero-order quadrature approximation of $\phi(u, v)$. Of course, the lower $(L_x L_y)/N$, the better the approximation.

It is seen that the radiators are more densely located where the reference current $i(x, y)$ is higher, leading to the expected spatial-density tapering. Also, even though radiators cannot be closer than $\min\{L_x/N_x, L_y/N_y\}$, their separation distances are commensurable. This entails the periodic (random) behavior of $\overline{F_1(u,v)}$. Hence, depending on L_x/N_x, L_y/N_y, and the level of thinning, grating lobes can enter the scan-range domain D. As a consequence, the bandwidth-steering product can be greatly reduced compared to aperiodic arrays [35].

IV. Statistically Thinned-Binned Arrays

In order to avoid grating lobes and thus enlarge the operational frequency band, the spacing between radiators must not be commensurable. To this end, a simple strategy is proposed: first, thinning is run, and then, a binning procedure follows. This new random array scheme is addressed as statistically thinned-binned arrays (STBAs).

More in detail, let us assume that statistical thinning is achieved so that the resulting array factor is provided by (3). Then, the locations of the element that survived the thinning are randomly perturbed as

$$\begin{aligned} x_n &= x_{nd} + \gamma_n \\ y_m &= y_{md} + \beta_m \end{aligned} \tag{10}$$

in which x_{nd} and y_{md} are the positions in the reference uniform grid, whereas $\{\gamma_n\}_{n=1}^{N_x}$ and $\{\beta_m\}_{m=1}^{N_y}$ are assumed to be

[independent and identically distributed (i.i.d.)] random variables uniformly distributed over $[-L_x/(2N_x), L_x/(2N_x)]$ and $[-L_y/(2N_y), L_y/(2N_y)]$ (i.e., the bin), respectively. Therefore, the resulting array factor can be written as

$$F_2(u,v) = C_2 \sum_{n=1}^{N_x}\sum_{m=1}^{N_y} F_{nm} e^{j\frac{2\pi}{\lambda}(x_n u + y_m v)} \tag{11}$$

where the final positions x_n and y_m are also random variables.

It is worth remarking that the choice of x_n and y_m coincides to the one used in the classic binned arrays [25]. However, as shown in [33], [34], [35], and [36], this scheme alone would not allow to shape the array factor. This drawback is, however, overcome by the joint use of the thinning procedure. Also, since $\{F_{nm}\}$ are real coefficients, as for STAs, the array factor is a Hermitian function, i.e., $F_2(-u,-v) = F_2^*(u,v)$, where * stands for complex conjugation.

Eventually, the random array is generated as follows. First, thinning is achieved by using the reference current in correspondence to the deterministic parts of x_n and y_n, that is, by setting $p_{nm} = \alpha[i(x_{nd}, y_{md})/\max\{i(x_{nd}, y_{md})\}]$. This procedure is equivalent to the classic STAs, and it allows to set the thinning independently of the random part of the radiators' positions. Then, radiators are deployed according to (10).

The corresponding average array factor is then given as (setting $C_2 = C_1$)]

$$\begin{aligned}
&\overline{F_2(u,v)} \\
&= C_2 \sum_{n=1}^{N_x}\sum_{m=1}^{N_y}\Bigg\{ p_{nm}\frac{N}{L_x L_y} \\
&\qquad \times \int_{x_{nd}-\frac{L_x}{2N_x}}^{x_{nd}+\frac{L_x}{2N_x}} \int_{y_{md}-\frac{L_y}{2N_y}}^{y_{md}+\frac{L_y}{2N_y}} e^{j\frac{2\pi}{\lambda}xu} e^{j\frac{2\pi}{\lambda}yv} dxdy \Bigg\} \\
&= \frac{L_x L_y}{N}\sum_{n=1}^{N_x}\sum_{m=1}^{N_y}\Bigg\{ i(x_{nd}, y_{md}) \\
&\qquad \times e^{j\frac{2\pi}{\lambda}(x_{nd}u + y_{nd}v)} \frac{\sin\left(\pi\frac{L_x}{\lambda N_x}u\right)}{\pi\frac{L_x}{\lambda N_x}u} \frac{\sin\left(\pi\frac{L_y}{\lambda N_y}v\right)}{\pi\frac{L_y}{\lambda N_y}v} \Bigg\}.
\end{aligned} \tag{12}$$

Equation (12) can be considered as a quadrature approximation of $\phi(u,v)$, but differently from (9), here only the relatively slowly varying $i(x,y)$ is approximated by a stepwise function. In particular, it is easy to verify that

$$\overline{F_2(u,v)} = \overline{F_1(u,v)}\,\mathrm{sinc}\left(\pi\frac{L_x}{\lambda N_x}u\right)\mathrm{sinc}\left(\pi\frac{L_y}{\lambda N_y}v\right) \tag{13}$$

from which it is readily seen that the sinc functions just forces zeros where grating lobes in $\overline{F_1(u,v)}$ could appear.

We conclude this section by observing that, for both STAs and STBAs, the number of radiators is described by the same random variable, namely

$$\nu = \sum_{n=1}^{N_x}\sum_{m=1}^{N_y} F_{nm}. \tag{14}$$

Since $\{F_{nm}\}$ are independent Bernoulli random variables, then ν is a Poisson binomial random variable whose mean and variance are given as

$$\bar{\nu} = \sum_{n=1}^{N_x}\sum_{m=1}^{N_y} p_{nm} \tag{15}$$

$$\sigma_\nu^2 = \bar{\nu^2} - \bar{\nu}^2 = \sum_{n=1}^{N_x}\sum_{m=1}^{N_y} p_{nm}(1-p_{nm}). \tag{16}$$

For large arrays, the number N is high. Hence, by Lyapunov's central limit theorem [37], ν can be considered Gaussian distributed, i.e., $\nu \sim \mathcal{N}(\bar{\nu}, \sigma_\nu^2)$. Accordingly,

$$P\{\bar{\nu} - 3\sigma_\nu \le \nu \le \bar{\nu} + 3\sigma_\nu\} = 99.7\%. \tag{17}$$

A. MSE Between the Actual and Reference Array Factors

So far, we have only discussed the new random array scheme from the point of view of the mean array factor. However, the average alone is insufficient to characterize a stochastic process. In order to capture how the array factor deviates from the desired one, the following MSE is considered:

$$\begin{aligned}
MSE_k(u,v) &= \overline{|F_k(u,v) - \phi(u,v)|^2} \\
&= \sigma_k^2(u,v) + |\overline{F_k(u,v)} - \phi(u,v)|^2
\end{aligned} \tag{18}$$

in which $\sigma_k^2(u,v)$ is the variance of the array factor and $k=1$ for STAs and $k=2$ for STBAs. In particular, for STAs, the variance is given by

$$\begin{aligned}
\sigma_1^2(u,v) &= \overline{|F_1(u,v)|^2} - |\overline{F_1(u,v)}|^2 \\
&= C_1^2 \sum_{n=1}^{N_x}\sum_{m=1}^{N_y} p_{nm}(1-p_{nm})
\end{aligned} \tag{19}$$

whereas, for STBAs, it is given by

$$\begin{aligned}
&\sigma_2^2(u,v) \\
&= \overline{|F_2(u,v)|^2} - \left|\overline{F_2(u,v)}\right|^2 \\
&= C_2^2 \sum_{n=1}^{N_x}\sum_{m=1}^{N_y} p_{nm}\left[1 - p_{nm}\left|\overline{e^{j\frac{2\pi}{\lambda}(x_n u + y_m v)}}\right|^2\right] \\
&= \left(\frac{L_x L_y}{\alpha N}\right)^2 \\
&\qquad \times \sum_{n=1}^{N_x}\sum_{m=1}^{N_y}\left\{ p_{nm}\left[1 - p_{nm}\left|\frac{\sin\left(\pi\frac{L_x}{\lambda N_x}u\right)}{\pi\frac{L_x}{\lambda N_x}u}\frac{\sin\left(\pi\frac{L_y}{\lambda N_y}v\right)}{\pi\frac{L_y}{\lambda N_y}v}\right|^2\right]\right\}.
\end{aligned} \tag{20}$$

As can be seen, while the variance of STAs is angle-independent, for STBAs, it is not true. Moreover, $\sigma_2^2(u,v) > \sigma_1^2(u,v)$, especially with u and v increasing. The latter represents the tradeoff for avoiding grating lobes. Indeed, the MSE pertaining to STAs is a periodic function (because $\overline{F_1(u,v)}$ is periodic), while for STBAs, the periodicity is lost.

From (18), it can be inferred that where $\phi(u,v) \approx 0$, the MSE equals the average power pattern, i.e., $MSE_k(u,v) \approx$

$\overline{P_k(u,v)} = \overline{|F_k(u,v)|^2} = |\overline{F_k(u,v)}|^2 + \sigma_k^2(u,v)$, with $P_k(u,v)$ being the power pattern. Furthermore, at points where the mean array factor is close to zero, both $MSE_k(u,v)$ and the mean power pattern are basically given by the variance of the array factor. Therefore, for STAs, the mean power pattern is given by (19), while for STBAs, it is given by (for u and v far from the origin)

$$\overline{|F_2(u,v)|^2} \approx \sigma_2^2(u,v) \approx \left(\frac{L_x L_y}{\alpha N}\right)^2 \sum_{n=1}^{N_x}\sum_{m=1}^{N_y} p_{nm}. \quad (21)$$

According to [5], when $|\overline{F_k(u,v)}|^2 \ll \sigma_k^2(u,v)$, the mean power pattern can also be called average statistical sidelobe (average value of the sidelobe) $\overline{SL}$. Unlike STAs, for STBAs, the parameter $\overline{SL}$ is a function of u and v. Furthermore, the average relative sidelobe level can be defined as (with $k = 1, 2$)

$$\delta_k \approx \frac{\sigma_k^2(u,v)}{|\overline{F_k(0,0)}|^2} \quad (22)$$

which represents an estimate of the peak sidelobe level of the average power pattern. According to the previous discussion, $\delta_k \approx MSE_k(u,v)/|\overline{F_k(0,0)}|^2$, where $\phi(u,v) \approx 0$ and $\overline{F_k(u,v)} \approx 0$.

B. Variance of the Power Pattern

To measure the dispersion of the power pattern around its mean, the power pattern variance is required. Remarkably, in the literature, little attention is paid to this parameter, and usually, the mean of the power pattern is mostly employed to characterize STAs [5].

To determine the variance of the power pattern, a methodology similar to the one used in [21] and [38] is considered. However, in the present article, the independence between the real and imaginary parts of the array factor is not needed. In particular, the variance of the power pattern is given as (subscript k is omitted for simplicity)

$$\begin{aligned}\sigma_P^2(u,v) &= \overline{P^2(u,v)} - \overline{P(u,v)}^2 \\ &= \overline{F_{\mathcal{R}}^4(u,v)} + \overline{F_{\mathcal{I}}^4(u,v)} + 2\overline{F_{\mathcal{R}}^2(u,v)F_{\mathcal{I}}^2(u,v)} \\ &\quad - \overline{F_{\mathcal{R}}^2(u,v)}^2 - \overline{F_{\mathcal{I}}^2(u,v)}^2 - 2\overline{F_{\mathcal{R}}^2(u,v)}\,\overline{F_{\mathcal{I}}^2(u,v)}\end{aligned} \quad (23)$$

in which $F_{\mathcal{R}}(u,v)$ and $F_{\mathcal{I}}(u,v)$ are the real and imaginary parts of the array factor, respectively. Since the number N is high, Lyapunov's central limit theorem [37] allows to consider, for each single (u,v), $F_{\mathcal{R}}(u,v)$, and $F_{\mathcal{I}}(u,v)$ as being jointly Gaussian random variables [1]. For this reason, considering the higher noncentral moments of a Gaussian random variable [39], (23) can be rewritten as follows (with (u,v) implied):

$$\begin{aligned}\sigma_P^2 &= \overline{P^2} - \overline{P}^2 \\ &= 4\mu_{\mathcal{R}}^2\sigma_{\mathcal{R}}^2 + 4\mu_{\mathcal{I}}^2\sigma_{\mathcal{I}}^2 + 2\sigma_{\mathcal{R}}^4 + 2\sigma_{\mathcal{I}}^4 - 2\mu_{\mathcal{R}}^2\mu_{\mathcal{I}}^2 \\ &\quad - 2\mu_{\mathcal{R}}^2\sigma_{\mathcal{I}}^2 - 2\mu_{\mathcal{I}}^2\sigma_{\mathcal{R}}^2 - 2\sigma_{\mathcal{R}}^2\sigma_{\mathcal{I}}^2 + 2\overline{F_{\mathcal{R}}^2F_{\mathcal{I}}^2}\end{aligned} \quad (24)$$

in which $\mu_{\mathcal{R}}(u,v)$ ($\mu_{\mathcal{I}}(u,v)$) and $\sigma_{\mathcal{R}}^2(u,v)$ ($\sigma_{\mathcal{I}}^2(u,v)$) are the mean and variance of the real (imaginary) part of the array factor (see the Appendix for relative details). To compute (24), $\overline{F_{\mathcal{R}}^2F_{\mathcal{I}}^2}$ must be determined. By Isserlis' theorem [40], it is obtained (with (u,v) implied)

$$\begin{aligned}\overline{F_{\mathcal{R}}^2F_{\mathcal{I}}^2} &= \overline{[(F_{\mathcal{R}} - \mu_{\mathcal{R}}) + \mu_{\mathcal{R}}]^2[(F_{\mathcal{I}} - \mu_{\mathcal{I}}) + \mu_{\mathcal{I}}]^2} \\ &= \sigma_{\mathcal{R}}^2\sigma_{\mathcal{I}}^2 + 2\mathcal{K}^2 + \mu_{\mathcal{I}}^2\sigma_{\mathcal{R}}^2 \\ &\quad + \mu_{\mathcal{R}}^2\sigma_{\mathcal{I}}^2 + \mu_{\mathcal{R}}^2\mu_{\mathcal{I}}^2 + 4\mu_{\mathcal{R}}\mu_{\mathcal{I}}\mathcal{K}\end{aligned} \quad (25)$$

in which $\mathcal{K}(u,v)$ represents the covariance function of $F_{\mathcal{R}}(u,v)$ and $F_{\mathcal{I}}(u,v)$ (see the Appendix).

Finally, (23)–(25) can be employed in conjunction with Cantelli's inequality [41] (with ξ being a real number)

$$\mathcal{P}_r\{P(u,v) \le \overline{P(u,v)} + \xi^2\} \ge 1 - \frac{\sigma_P^2(u,v)}{\sigma_P^2(u,v) + \xi^4} \quad (26)$$

to obtain a lower bound for the distribution of the power pattern, as a function of (u,v).

C. Distribution of the Power Pattern

Complete punctual (i.e., at a generic point (u,v)) characterization of the power pattern requires the cumulative distribution function. As previously stated, $F_{\mathcal{R}}(u,v)$ and $F_{\mathcal{I}}(u,v)$ can be considered jointly Gaussian. Hence, their joint density function can be written as (with (u,v) implied)

$$g(F_{\mathcal{R}}, F_{\mathcal{I}}) = \frac{e^{-\frac{1}{2(1-r^2)}\left[\frac{(F_{\mathcal{R}}-\mu_{\mathcal{R}})^2}{\sigma_{\mathcal{R}}^2} - 2r\frac{(F_{\mathcal{R}}-\mu_{\mathcal{R}})(F_{\mathcal{I}}-\mu_{\mathcal{I}})}{\sigma_{\mathcal{R}}\sigma_{\mathcal{I}}} + \frac{(F_{\mathcal{I}}-\mu_{\mathcal{I}})^2}{\sigma_{\mathcal{I}}^2}\right]}}{2\pi\sigma_{\mathcal{R}}\sigma_{\mathcal{I}}\sqrt{1-r^2}} \quad (27)$$

to which the following cumulative distribution function is associated:

$$\mathcal{P}_r\{P(u,v) \le \xi^2\} = \iint_{F_{\mathcal{R}}^2 + F_{\mathcal{I}}^2 \le \xi^2} g(F_{\mathcal{R}}, F_{\mathcal{I}})\, dF_{\mathcal{R}}\, dF_{\mathcal{I}}. \quad (28)$$

Unfortunately, to the best of authors' knowledge, (28) does not have a closed-form solution. However, at points (in the uv plane) where the mean of the array factor approaches the zero value, the variances of $F_{\mathcal{R}}(u,v)$ and $F_{\mathcal{I}}(u,v)$ assume the same values, and their correlation coefficient, $r(u,v)$, approaches zero (see the Appendix). Accordingly, (28) becomes a Rayleigh distribution.

A simplification is possible without invoking previous approximation if assuming that, for each radiator placed (initially) in (x_{nd}, y_{md}), with $\overline{F_{nm}} = p_{nm}$, there is another one placed in correspondence to $(-x_{nd}, -y_{md})$, with $\overline{F_{nm}} = p_{nm}$. This basically means assuming a certain symmetry for the reference current $i(x,y)$ and it entails that $\mu_{\mathcal{I}}(u,v) = r(u,v) = 0$. Note that steering is not impaired since the steering angle is already embodied within u and v.

Accordingly, (28) becomes a generalized noncentral chi-square distribution with two degrees of freedom [1], namely

$$\begin{aligned}&\mathcal{P}_r\{P(u,v) \le \xi^2\} \\ &\quad = \int_{-\xi}^{\xi}\int_{-\sqrt{\xi^2-F_{\mathcal{R}}^2}}^{\sqrt{\xi^2-F_{\mathcal{R}}^2}} \frac{e^{-\left[\frac{(F_{\mathcal{R}}-\mu_{\mathcal{R}})^2}{2\sigma_{\mathcal{R}}^2} + \frac{F_{\mathcal{I}}^2}{2\sigma_{\mathcal{I}}^2}\right]}}{2\pi\sigma_{\mathcal{R}}\sigma_{\mathcal{I}}} dF_{\mathcal{R}}\, dF_{\mathcal{I}}.\end{aligned} \quad (29)$$

Also, for this distribution, there is no closed-form expression, though some approximations can be found in the literature [42]. Moreover, it can be conveniently rewritten as

$$\mathcal{P}_r\{P(u,v) \le \xi^2\} = \int_{-\xi}^{\xi} \frac{e^{-\frac{(F_{\mathcal{R}}-\mu_{\mathcal{R}})^2}{2\sigma_{\mathcal{R}}^2}}}{\sqrt{2\pi}\sigma_{\mathcal{R}}} \left[1 - 2Q\left(\frac{\sqrt{\xi^2 - F_{\mathcal{R}}^2}}{\sigma_{\mathcal{I}}}\right)\right] dF_{\mathcal{R}} \quad (30)$$

with $Q(z) = (1/\sqrt{2\pi}) \int_z^{\infty} e^{-t^2/2} dt$ being the Q-function [39]. However, a numerical integration is still required for its computation. In order to obtain a more tractable expression, we also assume that $\sigma_{\mathcal{I}}^2(u,v) \approx \sigma_{\mathcal{R}}^2(u,v)$. Note that this is similar to the assumption made in [43], and it is at least reasonable far from the main beam of the array factor (see the Appendix for details). Also, by considering $P(u,v)/\sigma_{\mathcal{R}}^2(u,v)$, which is now a noncentral chi-square random variable with two degrees of freedom, we obtain

$$\begin{aligned}\mathcal{P}_r\left\{\frac{P(u,v)}{\sigma_{\mathcal{R}}^2(u,v)} \le \xi^2\right\} &\approx \int_0^{\xi}\int_0^{2\pi} \frac{e^{-\left[\frac{\{A\cos\gamma - (\mu_{\mathcal{R}}/\sigma_{\mathcal{R}})\}^2}{2} + \frac{(A\sin\gamma)^2}{2}\right]}}{2\pi} A\,dA\,d\gamma \\ &= \int_0^{\xi} A e^{-\frac{A^2 + (\mu_{\mathcal{R}}/\sigma_{\mathcal{R}})^2}{2}} I_0\left(\frac{A\mu_{\mathcal{R}}}{\sigma_{\mathcal{R}}}\right) dA \\ &= 1 - \mathrm{Q}_1\left(\sqrt{\tau}, \xi\right) \end{aligned} \quad (31)$$

in which the term I_0 is the modified Bessel function of zero order, $\mathrm{Q}_1(a,b)$ is the Marcum Q-function [44] of order 1, and $\tau = \mu_{\mathcal{R}}^2(u,v)/\sigma_{\mathcal{R}}^2(u,v) \ge 0$ is the so-called noncentrality parameter [39].

Equation (31) allows to easily obtain a more general probability characterization of the power pattern. For example, it can be set $\mathcal{P}_r\{[P(u,v)/\sigma_{\mathcal{R}}^2(u,v)] \le \mathcal{LS}_{\eta}^2(u,v)\} = \eta\%$ and find an estimation of the η-percent level surface, $\mathcal{LS}_{\eta}^2(u,v)$. This procedure is further simplified if looking at an approximate solution. Indeed, for a noncentral chi-square distribution with two degrees of freedom, the percentile curves can be easily determined by means of the following approximation [39]:

$$\mathcal{LS}_{\eta}^2(u,v) \approx a\left[x_{\eta}\sqrt{\frac{2}{9}\left(\frac{1+b}{a}\right)} + 1 - \frac{2}{9}\left(\frac{1+b}{a}\right)\right]^3 \quad (32)$$

in which $a = 2 + \tau$, $b = \tau/(2+\tau)$, and x_{η} is the ηth percentile of the standardized Gaussian random variable. It is worth emphasizing that (32) allows to calculate the percentiles of the power pattern, for each (u,v), without the need to perform any inversion [as for (31)]. In fact, it is enough to know the mean and the variance of the real part of the array factor. Obviously, $\mathcal{LS}_{\eta}^2(u,v)$ represents the ηth percentile of $P(u,v)/\sigma_{\mathcal{R}}^2(u,v)$. Accordingly, $\mathcal{LS}_{\eta}^2(u,v) \cdot \sigma_{\mathcal{R}}^2(u,v)$ is the ηth percentile of $P(u,v)$.

Finally, it is noted that, as discussed in Section IV-B, also Cantelli's inequality (26) can be used to obtain an upper bound estimation of $\mathcal{LS}_{\eta}^2(u,v)$. Indeed, Cantelli's inequality is valid under a more general framework than (32) since it does not require to assume the mentioned symmetry for $i(x,y)$ nor to consider $\sigma_{\mathcal{I}}^2(u,v) = \sigma_{\mathcal{R}}^2(u,v)$. However, it is expected to return a less sharp bound, and this justifies the derivation of (32).

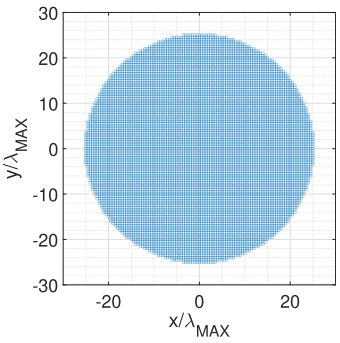

Fig. 1. Reference filled array.

V. Numerical Results

In this section, some numerical results are shown in order to check the presented theoretical arguments. To this end, $i(x,y)$ is chosen according to the Hansen design for circular apertures [45]. The reference filled array is a uniform half-wavelength (at the minimum operating frequency, i.e., for $\lambda = \lambda_{MAX}$) square grid, as in [5], where only elements inside the circle inscribed in the square grid are retained. For example, Fig. 1 shows a filled array with $N = 8021$.

The results are presented along the cuts of the array factor, at the maximum operating frequency (i.e., for $\lambda = \lambda_{min}$). More in detail, defining $u = \rho\cos\gamma$ and $v = \rho\sin\gamma$, with $\rho \in [0,2]$, each cut refers to a given fixed γ. Since the array factor is Hermitian, it suffices to fix γ within the interval $(-\pi/2, \pi/2]$. Along a generic cut, the array factor is sampled with a step equal to $\Delta\rho = \lambda_{min}/(8L_x)$. This means that along the u-axis ($\gamma = 0$) and v-axis ($\gamma = \pi/2$), the sampling step is four times finer than the Nyquist step for the power pattern.

Fig. 2 shows a naturally (i.e., $\alpha = 1$) thinned STBA realization starting from the array in Fig. 1 and employing the Hansen design with parameter $H = 1.1977 \Rightarrow sll_{dB} = -30$ dB. The remaining antenna elements are $3612 \approx 45\%N$. As expected from the Hansen reference current, the elements are mainly concentrated toward the array center. In Fig. 2, the normalized magnitude of the array factors corresponding to the reference array ($\widetilde{\phi}(\rho,\gamma)_{dB} = 20\log_{10}\{|\phi(\rho,\gamma)|/|\phi(0,0)|\}$), to an STA realization ($\widetilde{F}_1(\rho,\gamma)_{dB} = 20\log_{10}\{|F_1(\rho,\gamma)|/|F_1(0,0)|\}$), and to an STBA realization ($\widetilde{F}_2(\rho,\gamma)_{dB} = 20\log_{10}\{|F_2(\rho,\gamma)|/|F_2(0,0)|\}$) is compared for three different cuts and $f_{MAX} = 5f_{min}$ (with f_{min} and f_{MAX} being the minimum and maximum operating frequencies, respectively). As can be seen, the near-in sidelobes of both STAs and STBAs are similar to those of the reference array factor. Far away from the main lobe, sidelobes increase, although they do not exceed -27 dB. This is worth noting since the actual goal of thinned arrays is to obtain a peak sidelobe level as close as possible to that of the reference array factor, rather than to mimic the reference pattern behavior. What is more, while $\widetilde{F}_2(\rho,\gamma)_{dB}$ does not present grating lobes, $\widetilde{F}_1(\rho,\gamma)_{dB}$ does. Therefore, the broadband nature of the STBAs is evident. Note that the STA grating lobe periodicity is not the same in each cut since periodicity occurs along the u- and v-axes. Fig. 3 offers a

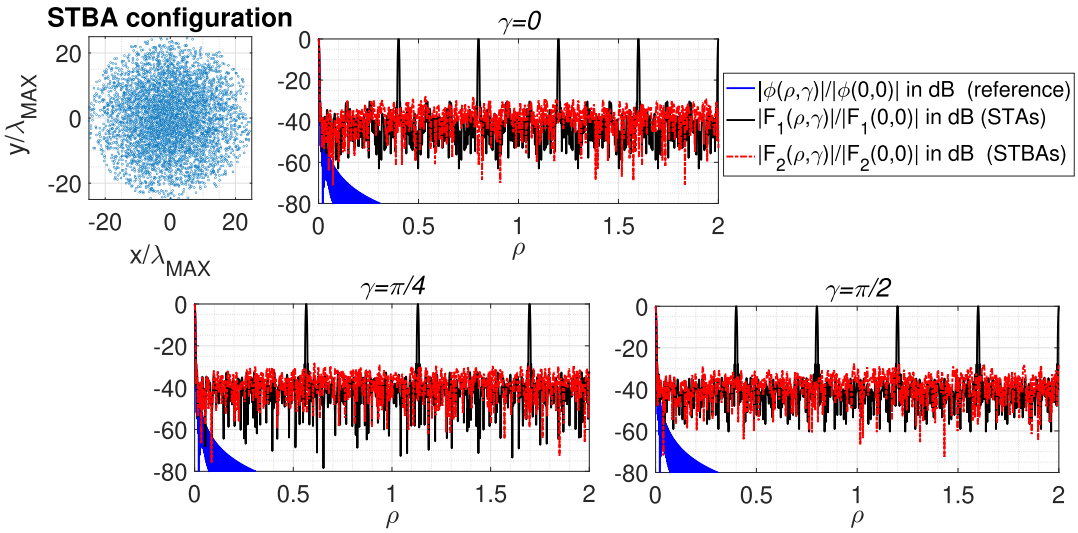

Fig. 2. Geometry of a realization of STBA; comparison, for different cuts, between the magnitude of the reference array factor and the realizations of the array factor magnitude of STA and the array factor magnitude of STBA. The reference current is given by the Hansen design for circular apertures with a sidelobe level of -30 dB. The initial number of elements is $N = 8021$ and $\alpha = 1$ (natural thinning). The bandwidth is 5:1.

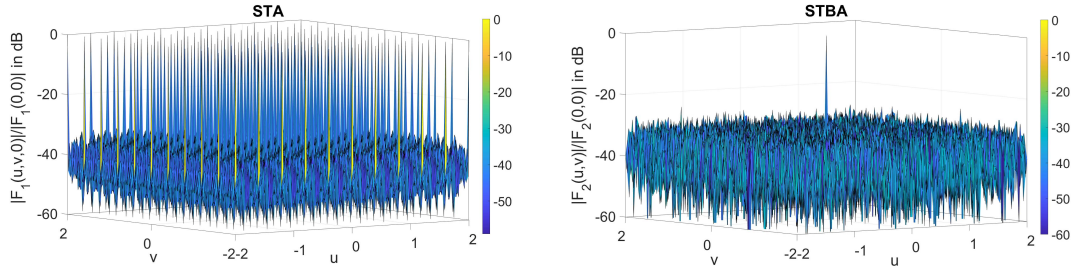

Fig. 3. 3-D view of the normalized (a) STA and (b) STBA array factor magnitude realizations for the case of Fig. 2.

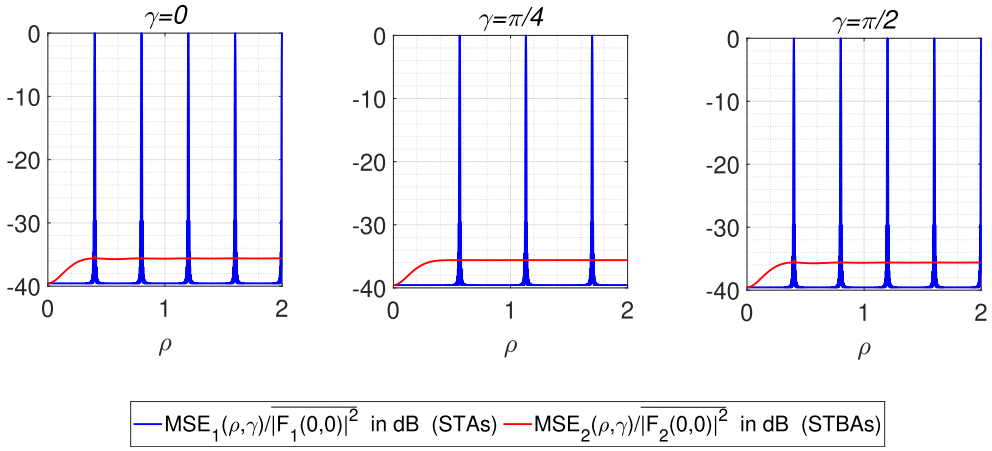

Fig. 4. Normalized MSE behavior for the case of Fig. 2.

3-D view of STA and STBA realizations, which allows to better appreciate how STBAs are free from grating lobes.

In Fig. 4, the previous example is addressed from the perspective provided by $MSE_1(\rho,\gamma)/\overline{|F_1(0,0)|^2}$ and $MSE_2(\rho,\gamma)/\overline{|F_2(0,0)|^2}$. As can be seen, in both cases, the MSE is very low in the main-lobe region ($\rho \simeq 0$). In the sidelobe region, the normalized MSE of STBAs approaches the array factor variance and keeps nearly constant, whereas for STAs, though it is lower in between grating lobes, the MSE reaches almost 0 dB at the grating lobes of the array factor. In other words, far from the main lobe, while for STBAs, the sidelobes mainly depend on the array factor variances, for

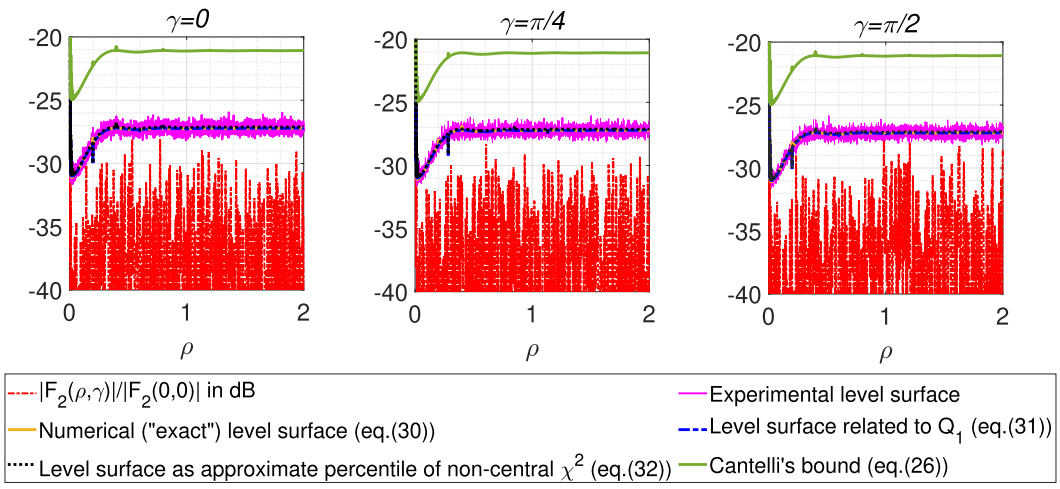

Fig. 5. Cuts of the (normalized) 99.9% level surfaces related to the configuration of Fig. 2. The curves are related to STBAs only.

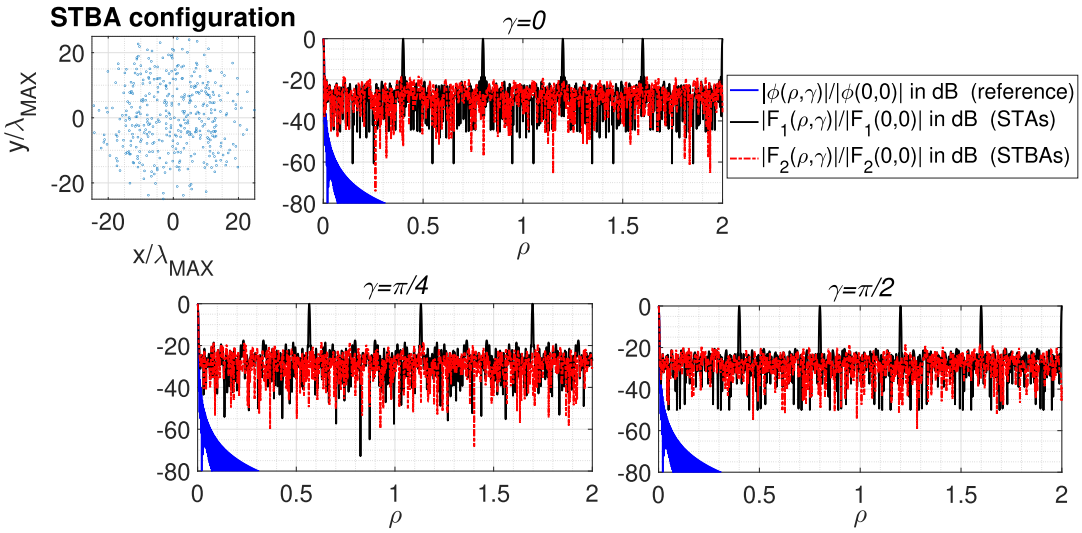

Fig. 6. Geometry of a realization of STBA; comparison, for different cuts, between the magnitude of the reference array factor and the realizations of the array factor magnitude of STA and the array factor magnitude of STBA. The reference current is given by the Hansen design for circular apertures with a sidelobe level of -30 dB. The initial number of elements is $N = 8021$ and $\alpha = 0.1103$ ($\approx 95\%$ of thinning). The bandwidth is 5:1.

STAs, they are affected by both the variance and the mean of the array factor, the latter being periodic.

By comparing Figs. 2 and 4, it is also evident that the variance of the array factor (i.e., the mean power pattern), which is often used to estimate the behavior of sidelobes, generally returns underestimated (optimistic) values.

Fig. 2 refers to single array realizations, and hence, it is not sufficient to give a statistical array characterization. To cope with this issue, of course only for STBAs, we consider the percentile curves. In particular, we compare the upper bound arising from (26) and the outcomes provided by (31) and its approximation (32). The corresponding three 99.9%-percentile curves are compared to the results returned by a Monte Carlo "experimental" analysis in Fig. 5. In particular, such a figure shows a comparison along the three considered cuts of the normalized (to $\overline{P_2(0,0)} = \overline{|F_2(0,0)|^2}$) 99.9% level surfaces. Also, the experimental percentile curve has been obtained by running a Monte Carlo simulation with 4000 trials for each ρ. It is worth specifying that the estimated level surfaces have been normalized by $\overline{P_2(0,0)}$. This simplifies the matter, by avoiding to consider the random nature of the normalizing factor. This procedure is actually justified since the coefficient of variation of the power pattern, $CV(u,v,) = \sigma_P(u,v)/\overline{P_2(u,v)}$, is minimum at $(u,v) = (0,0)$. Accordingly, $P_2(0,0)$ can be approximated by $\overline{P_2(0,0)}$ [21]. Nonetheless, the realization of the power pattern has been obtained by normalizing $P_2(u,v)$ by $P_2(0,0)$.

It is seen that Cantelli's inequality actually returns an upper bound, which, however, is not very sharp. Instead, the percentile curves given by (31) and (32) are practically overlapping and, what is more, they are very close to the experimental curve. Accordingly, it is concluded that both (31) and (32)

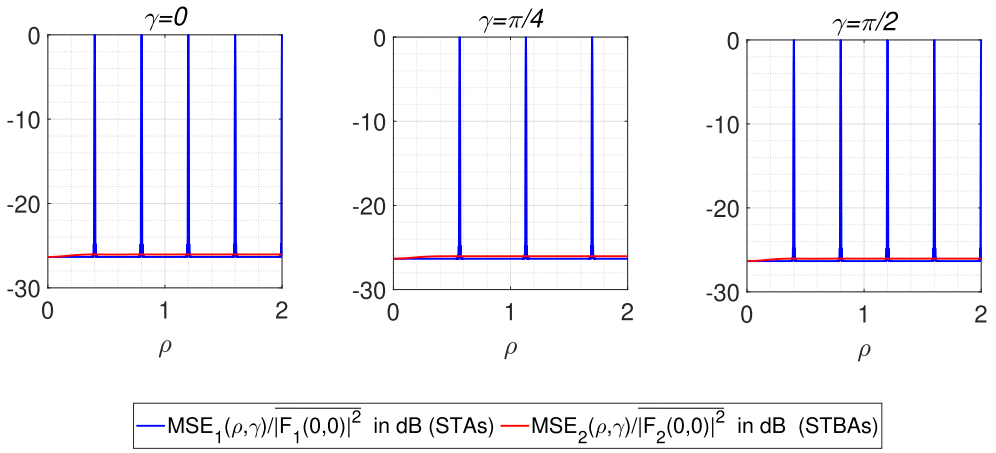

Fig. 7. Normalized mean squared error between the actual and reference array factors for STAs and STBAs for the configuration of Fig. 6.

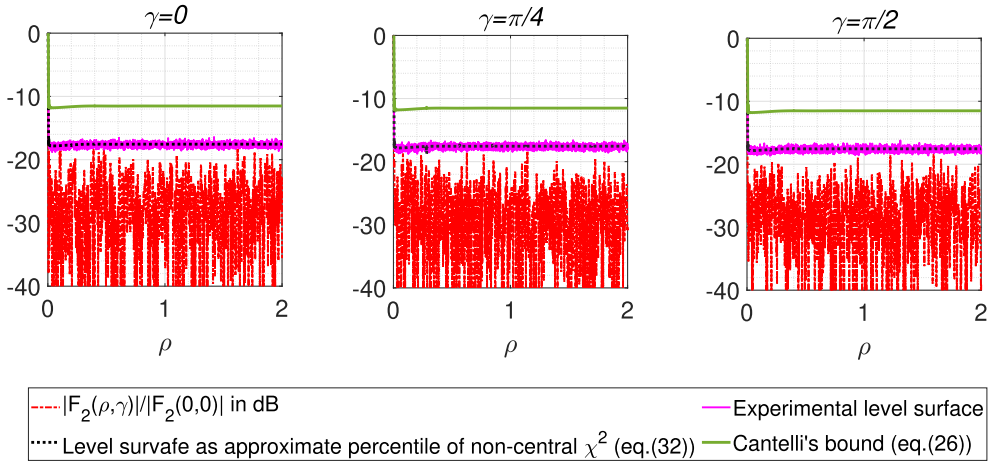

Fig. 8. Cuts of the (normalized) 99.9% level surfaces related to the configuration of Fig. 6. The curves are related to STBAs only.

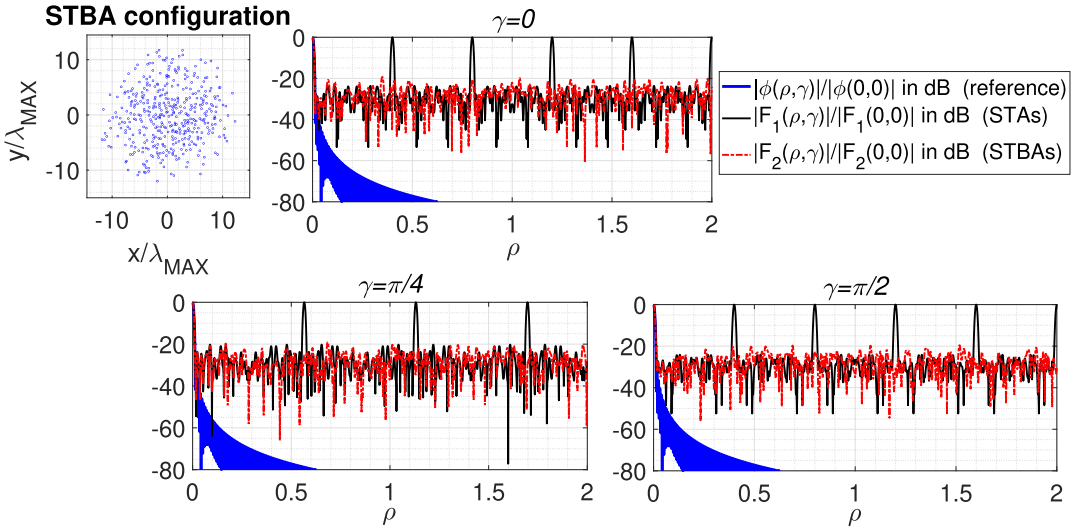

Fig. 9. Geometry of a realization of STBA; comparison, for different cuts, between the magnitude of the reference array factor and the realizations of the array factor magnitude of STA and the array factor magnitude of STBA. The reference current is given by the Hansen design for circular apertures with a sidelobe level of -30 dB. The initial number of elements is $N = 1976$ and $\alpha = 0.4466$ ($\approx 80\%$ of thinning). The bandwidth is 5:1.

can be used to foresee the power pattern behavior, but (32) is preferable because of its simplicity of implementation (no inversion is required). Hence, hereinafter, we will be considering only the estimation provided by (32). Cantelli's

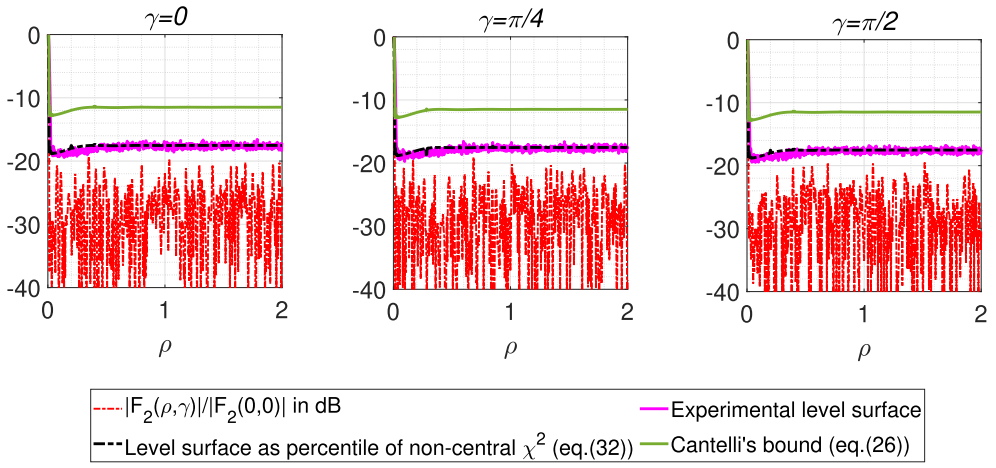

Fig. 10. Cuts of the (normalized) 99.9% level surfaces related to the configuration of Fig. 9. The curves are related to STBAs only.

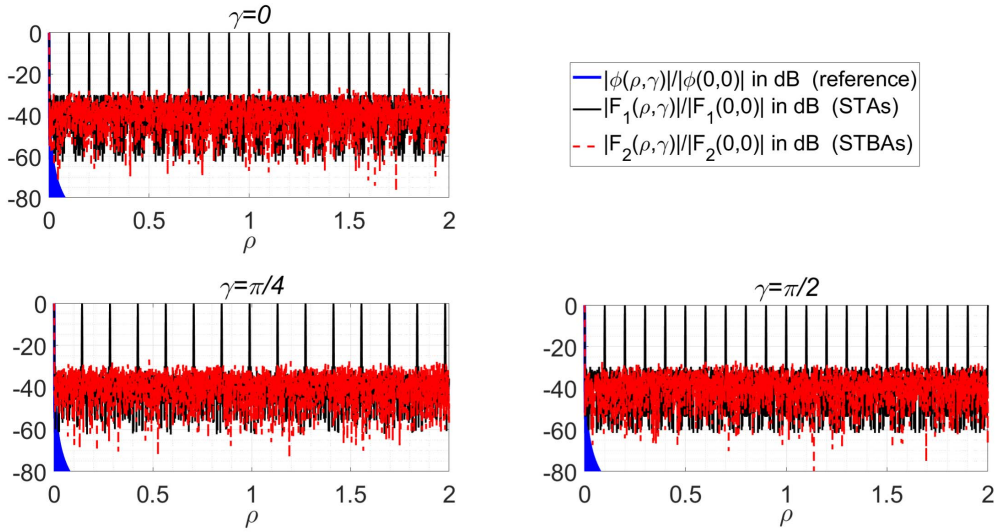

Fig. 11. Comparison, for different cuts, between the magnitude of the reference array factor and realizations of the array factor magnitude of STA and the array factor magnitude of STBA. The reference current is given by the Hansen design for circular apertures with a sidelobe level of -30 dB. The initial number of elements is $N = 8021$ and $\alpha = 1$ (natural thinning). The bandwidth is 20:1.

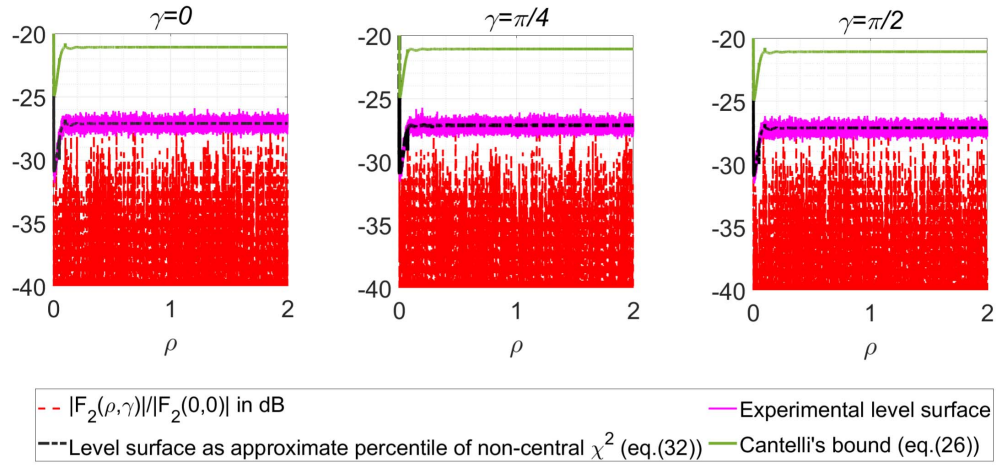

Fig. 12. Cuts of the (normalized) 99.9% level surface related to the configuration of Fig. 11. The curves are related to STBAs only.

bound instead is a good option to be used in a more general framework when the hypotheses behind (32) are not met.

The previous example actually showed the broadband nature of the proposed STBAs scheme and the effectiveness of the

theoretical tools to foresee the power pattern behavior. Now, some selected further examples are presented, following the same rationale as above, to complete the picture.

We start by rerunning the previous case, but forcing a very stringent thinning, so that the reduction of antenna elements is equal about to 95%. The results for this case are reported in Figs. 6–8. As can be seen, the STBA realization has a much smaller number of antenna elements, $412 \approx 5\% N$ and the sidelobes increase. This is actually expected, since it is well known that, for aperiodic arrays, the sidelobes strongly depend on the number of antenna elements [1], [3], [4], [35]. However, STBAs still do not present grating lobes (unlike STAs). Also, it is seen once more that the mean power pattern does not return a reliable sidelobe estimation (see Fig. 7), whereas the theoretical percentile curve estimations work very well.

The next example is shown in Figs. 9 and 10, and it refers to a smaller array. More in detail, the filled array consists of $N = 1976$, whereas, after the thinning ($\alpha = 0.4466$), roughly 20% of the elements remain. Note that the thinning level has been chosen so as to have approximately the same elements in the array, as for example, in Fig. 6. From this last example, the broadband nature of STBAs is evident again. Also, the theoretical predictions are still very good. Finally, the peak sidelobe level behavior is practically the same as in the previous case, confirming the role played by the actual number of elements in the array.

As mentioned earlier (and confirmed by the numerical analysis), the STBAs scheme inherits the ability to work on very wide frequency bands. To further check this statement, in Figs. 11 and 12, a case with the same setup as in Fig. 2, but with a 20:1 bandwidth, is considered. Even for this extremely large frequency band, STBAs sidelobes show quite low levels, around the same value as in Fig. 2. Instead, the STAs' patterns have a higher number of grating lobes, due to the increased bandwidth. This definitely proves the excellent frequency behavior of STBAs, by confirming the proposed theory as a tool to a priori foresee the array behavior and to properly select the parameters according to possible design specifications.

VI. Conclusion

In this article, a new and simple approach for obtaining random arrays has been introduced.

It basically consists in pairing two classical schemes: the statistical thinning and the binned strategy. Accordingly, this scheme has been termed STBAs. The proposed strategy inherits the positive features of the merged schemes. Indeed, the number of elements is reduced, as in the classical thinning but, due to the binning procedure, the elemental radiators that survived the thinning are not separated by commensurable distances. Thus, the array factor is no longer periodic and grating lobes are avoided. Finally, the proposed strategy presents some advantages over the totally random arrays as well. Indeed, because of the binning stage, the radiators tend to more uniformly fill the array aperture, which leads to a higher average separation between the elements and, ultimately, to better exploit the available aperture.

In order to foresee the statistical features of the proposed random array scheme, the study addressed some theoretical aspects that, for example, allowed to find closed-form estimations for the percentile-level surfaces in terms of the parameters of the array. The selected numerical analysis clearly shows that STBAs exhibit broadband behavior, without the appearance of grating lobes. Also, the theoretical estimations are in excellent agreement with the Monte Carlo analysis. This is extremely relevant since the closed-form expressions give a direct link between the array parameters and its statistical features. Hence, they can be exploited for analysis but also for synthesis purposes.

Appendix
Moments, Covariance, and Correlation Coefficient of $F_{\mathcal{R}}(u,v)$ and $F_{\mathcal{I}}(u,v)$

Considering STBA, $\mu_{\mathcal{R}}(u,v)$ and $\mu_{\mathcal{I}}(u,v)$ are the real and imaginary parts of (12), respectively, i.e.,

$$\mu_{\mathcal{R}}(u,v) = C_2 \frac{\sin\left(\frac{\pi}{\lambda} L_x u\right)}{\frac{\pi}{\lambda N_x} L_x u} \frac{\sin\left(\frac{\pi}{\lambda N_y} L_y v\right)}{\frac{\pi}{\lambda N_y} L_y v} \times \sum_{n=1}^{N_x} \sum_{m=1}^{N_y} p_{nm} \cos\left[\frac{2\pi}{\lambda}(x_{nd} u + y_{md} v)\right] \quad (33)$$

$$\mu_{\mathcal{I}}(u,v) = C_2 \frac{\sin\left(\frac{\pi}{\lambda N_x} L_x u\right)}{\frac{\pi}{\lambda N_x} L_x u} \frac{\sin\left(\frac{\pi}{\lambda N_y} L_y v\right)}{\frac{\pi}{\lambda N_y} L_y v} \times \sum_{n=1}^{N_x} \sum_{m=1}^{N_y} p_{nm} \sin\left[\frac{2\pi}{\lambda}(x_{nd} u + y_{md} v)\right]. \quad (34)$$

Hence, the variances of $F_{\mathcal{R}}(u,v)$ and $F_{\mathcal{I}}(u,v)$ readily arise as

$$\begin{aligned}\sigma^2_{\mathcal{R}}(u,v) = {} & \frac{C_2^2}{2} \sum_{n=1}^{N_x} \sum_{m=1}^{N_y} p_{nm} \\ & + \frac{C_2^2}{2} \frac{\sin\left(\frac{2\pi}{\lambda N_x} L_x u\right)}{\frac{2\pi}{\lambda N_x} L_x u} \frac{\sin\left(\frac{2\pi}{\lambda N_y} L_y v\right)}{\frac{2\pi}{\lambda N_y} L_y v} \\ & \times \sum_{n=1}^{N_x} \sum_{m=1}^{N_y} p_{nm} \cos\left[\frac{4\pi}{\lambda}(x_{nd} u + y_{md} v)\right] \\ & - C_2^2 \left[\frac{\sin\left(\frac{\pi}{\lambda N_x} L_x u\right)}{\frac{\pi}{\lambda N_x} L_x u} \frac{\sin\left(\frac{\pi}{\lambda N_y} L_y v\right)}{\frac{\pi}{\lambda N_y} L_y v}\right]^2 \\ & \times \sum_{n=1}^{N_x} \sum_{m=1}^{N_y} p_{nm}^2 \cos^2\left[\frac{2\pi}{\lambda}(x_{nd} u + y_{md} v)\right] \end{aligned} \quad (35)$$

$$\begin{aligned}\sigma^2_{\mathcal{I}}(u,v) = {} & \frac{C_2^2}{2} \sum_{n=1}^{N_x} \sum_{m=1}^{N_y} p_{nm} \\ & - \frac{C_2^2}{2} \frac{\sin\left(\frac{2\pi}{\lambda N_x} L_x u\right)}{\frac{2\pi}{\lambda N_x} L_x u} \frac{\sin\left(\frac{2\pi}{\lambda N_y} L_y v\right)}{\frac{2\pi}{\lambda N_y} L_y v} \\ & \times \sum_{n=1}^{N_x} \sum_{m=1}^{N_y} p_{nm} \cos\left[\frac{4\pi}{\lambda}(x_{nd} u + y_{md} v)\right] \end{aligned}$$

$$- C_2^2 \left[\frac{\sin\left(\frac{\pi}{\lambda N_x} L_x u\right)}{\frac{\pi}{\lambda N_x} L_x u} \frac{\sin\left(\frac{\pi}{\lambda N_y} L_y v\right)}{\frac{\pi}{\lambda N_y} L_y v} \right]^2 \times \sum_{n=1}^{N_x} \sum_{m=1}^{N_y} p_{nm}^2 \sin^2\left[\frac{2\pi}{\lambda} (x_{nd} u + y_{md} v) \right]. \quad (36)$$

It can be easily recognized that $\sigma_{\mathcal{R}}^2(u,v) + \sigma_{\mathcal{I}}^2(u,v) = \sigma_2^2(u,v)$, as it must be.

The covariance function of $F_{\mathcal{R}}(u,v)$ and $F_{\mathcal{I}}(u,v)$ is then given by

$$\mathcal{K}(u,v) = \frac{C_2^2}{2} \frac{\sin\left(\frac{2\pi}{\lambda N_x} L_x u\right)}{\frac{2\pi}{\lambda N_x} L_x u} \frac{\sin\left(\frac{2\pi}{\lambda N_y} L_y v\right)}{\frac{2\pi}{\lambda N_y} L_y v} \times \sum_{n=1}^{N_x} \sum_{m=1}^{N_y} p_{nm} \sin\left[\frac{4\pi}{\lambda} (x_{nd} u + y_{md} v) \right] - \frac{C_2^2}{2} \left[\frac{\sin\left(\frac{\pi}{\lambda N_x} L_x u\right)}{\frac{\pi}{\lambda N_x} L_x u} \frac{\sin\left(\frac{\pi}{\lambda N_y} L_y v\right)}{\frac{\pi}{\lambda N_y} L_y v} \right]^2 \times \sum_{n=1}^{N_x} \sum_{m=1}^{N_y} p_{nm}^2 \sin\left[\frac{4\pi}{\lambda} (x_{nd} u + y_{md} v) \right]. \quad (37)$$

Finally, the Bravais–Pearson correlation coefficient of the quadrature components is given as: $r(u,v) = \mathcal{K}(u,v) / [\sigma_{\mathcal{R}}(u,v)\sigma_{\mathcal{I}}(u,v)]$.

It can be easily checked that, if for each radiator placed in (x_{nd}, y_{md}), there is another one located in $(-x_{nd}, -y_{md})$, and they both have the same coefficient p_{nm}, then $\mu_{\mathcal{I}}(u,v)$, $\mathcal{K}(u,v)$, and $r(u,v)$ are zero everywhere.

REFERENCES

[1] Y. T. Lo, "A mathematical theory of antenna arrays with randomly spaced elements," *IEEE Trans. Antennas Propag.*, vol. AP-12, no. 3, pp. 257–268, May 1964.

[2] A. Ishimaru and Y.-S. Chen, "Thinning and broadbanding antenna arrays by unequal spacings," *IEEE Trans. Antennas Propag.*, vol. AP-13, no. 1, pp. 34–42, Jan. 1965.

[3] B. D. Steinberg, "The peak sidelobe of the phased array having randomly located elements," *IEEE Trans. Antennas Propag.*, vol. AP-20, no. 2, pp. 129–136, Mar. 1972.

[4] G. Buonanno and R. Solimene, "Comparing different schemes for random arrays," *Prog. Electromagn. Res. B*, vol. 71, pp. 107–118, 2016.

[5] M. I. Skolnik, J. Sherman, and F. Ogg Jr., "Statistically designed density-tapered arrays," *IEEE Trans. Antennas Propag.*, vol. AP-12, no. 4, pp. 408–417, Jul. 1964.

[6] R. J. Mailloux, *Phased Array Antenna Handbook* (Artech House Antennas and Propagation Library), 2nd ed. Norwood, MA, USA: Artech House, 2005.

[7] R. L. Haupt, "Adaptively thinned arrays," *IEEE Trans. Antennas Propag.*, vol. 63, no. 4, pp. 1626–1632, Apr. 2015.

[8] F. Boulos et al., "A computational inversion method for interference suppression in reconfigurable thinned ring arrays," *J. Phys., Conf.* vol. 1476, May 2020, Art. no. 012016, doi: 10.1088/1742-6596/1476/1/012016.

[9] R. L. Haupt, *Antenna Arrays: A Computational Approach*. Hoboken, NJ, USA: Wiley-IEEE Press, 2010.

[10] R. L. Haupt, "Thinned arrays using genetic algorithms," *IEEE Trans. Antennas Propag.*, vol. 42, no. 7, pp. 993–999, Jul. 1994.

[11] A. T. V. Murino and C. S. Regazzoni, "Synthesis of unequally spaced arrays by simulated annealing," *IEEE Trans. Signal Process.*, vol. 44, no. 1, pp. 119–123, Jan. 1996.

[12] M. M. Khodier and C. G. Christodoulou, "Linear array geometry synthesis with minimum sidelobe level and null control using particle swarm optimization," *IEEE Trans. Antennas Propag.*, vol. 53, no. 8, pp. 2674–2679, Aug. 2005.

[13] N. Jin and Y. Rahmat-Samii, "Advances in particle swarm optimization for antenna designs: Real-number, binary, single-objective and multiobjective implementations," *IEEE Trans. Antennas Propag.*, vol. 55, no. 3, pp. 556–567, Mar. 2007.

[14] O. Quevedo-Teruel and E. Rajo-Iglesias, "Ant colony optimization in thinned array synthesis with minimum sidelobe level," *IEEE Antennas Wireless Propag. Lett.*, vol. 5, pp. 349–352, 2006.

[15] S. K. Goudos and J. N. Sahalos, "Design of large thinned arrays using different biogeography-based optimization migration models," *Int. J. Antennas Propag.*, vol. 2016, pp. 1–11, Sep. 2016, doi: 10.1155/2016/5359298.

[16] W. P. M. N. Keizer, "Large planar array thinning using iterative FFT techniques," *IEEE Trans. Antennas Propag.*, vol. 57, no. 10, pp. 3359–3362, Oct. 2009.

[17] W. P. M. N. Keizer, "Synthesis of thinned planar circular and square arrays using density tapering," *IEEE Trans. Antennas Propag.*, vol. 62, no. 4, pp. 1555–1563, Apr. 2014.

[18] X.-K. Wang, Y.-C. Jiao, and Y.-Y. Tan, "Synthesis of large thinned planar arrays using a modified iterative Fourier technique," *IEEE Trans. Antennas Propag.*, vol. 62, no. 4, pp. 1564–1571, Apr. 2014.

[19] E. Tohidi, M. M. Nayebi, and H. Behroozi, "Dynamic programming applied to large circular arrays thinning," *IEEE Trans. Antennas Propag.*, vol. 66, no. 8, pp. 4025–4033, Aug. 2018.

[20] R. J. Mailloux and E. Cohen, "Statistically thinned arrays with quantized element weights," *IEEE Trans. Antennas Propag.*, vol. 39, no. 4, pp. 436–447, Apr. 1991.

[21] G. Buonanno and R. Solimene, "Global characterization of linear statistically thinned antenna arrays," *IEEE Access*, vol. 9, pp. 119629–119640, 2021.

[22] G. Buonanno, S. Costanzo, and R. Solimene, "Statistically thinned array antennas for simultaneous multibeam applications," *IEEE Access*, vol. 10, pp. 60230–60240, 2022.

[23] T. Numazaki, S. Mano, T. Kategi, and M. Mizusawa, "An improved thinning method for density tapering of planar array antennas," *IEEE Trans. Antennas Propag.*, vol. AP-35, no. 9, pp. 1066–1069, Sep. 1987.

[24] Y. T. Lo, "Random periodic arrays," *Radio Sci.*, vol. 3, no. 5, pp. 425–436, May 1968.

[25] W. J. Hendricks, "The totally random versus the bin approach for random arrays," *IEEE Trans. Antennas Propag.*, vol. 39, no. 12, pp. 1757–1762, Dec. 1991.

[26] K. Buchanan and G. H. Huff, "A stochastic mathematical framework for the analysis of spherically-bound random arrays," *IEEE Trans. Antennas Propag.*, vol. 62, no. 6, pp. 3002–3011, Jun. 2014.

[27] G. Buonanno and R. Solimene, "Unequally excited generalised random binned antenna arrays," *IET Microw., Antennas Propag.*, vol. 13, no. 14, pp. 2531–2538, Nov. 2019.

[28] R. E. Willey, "Space tapering of linear and planar arrays," *IRE Trans. Antennas Propag.*, vol. 10, no. 4, pp. 369–377, Jul. 1962.

[29] F. Venneri, S. Costanzo, G. Di Massa, A. Borgia, P. Corsonello, and M. Salzano, "Design of a reconfigurable reflectarray based on a varactor tuned element," in *Proc. 6th Eur. Conf. Antennas Propag. (EUCAP)*, Mar. 2012, pp. 2628–2631.

[30] F. Venneri et al., "Beam-scanning reflectarray based on a single varactor-tuned element," *Int. J. Antennas Propag.*, vol. 2012, Jun. 2012, Art. no. 290285, doi: 10.1155/2012/290285.

[31] D. M. Pozar, *Microwave Engineering*, 4th ed. Hoboken, NJ, USA: Wiley, 2011.

[32] S. Costanzo, "Synthesis of multi-step coplanar waveguide-to-microstrip transition," *Prog. Electromagn. Res.*, vol. 113, pp. 111–126, 2011.

[33] G. Buonanno and R. Solimene, "Generalised random binned antenna arrays," *Prog. Electromagn. Res. C*, vol. 78, pp. 129–143, 2017.

[34] V. D. Agrawal and Y. T. Lo, "Distribution of sidelobe level in random arrays," *Proc. IEEE*, vol. 57, no. 10, pp. 1764–1765, Oct. 1969.

[35] M. Andreasen, "Linear arrays with variable interelement spacings," *IRE Trans. Antennas Propag.*, vol. 10, no. 2, pp. 137–143, Mar. 1962.

[36] G. Buonanno and R. Solimine, "Probabilistic density-tapered antenna arrays," in *Proc. Prog. Electromagn. Res. Symp. (PIERS-Toyama)*, Toyama, Japan, 2018, pp. 1–4.

[37] H. Cramér and M. R. Leadbetter, *Stationary and Related Stochastic Processes: Sample Function Properties and Their Applications*. New York, NY, USA: Dover, 2004.

[38] K. Buchanan et al., "Analysis of collaborative beamforming for circularly bound random antenna array distributions," Nav. Inf. Warfare Center Pacific (NIWC Pacific), San Diego, CA, USA, Tech. Rep. 3218, Nov. 2020.

[39] M. Zelen and N. C. Severo, "Probability functions," in *Handbook of Mathematical Functions With Formulas, Graphs and Mathematical Tables* (National Bureau of Standards Applied Mathematics Serie), no. 55, M. Abramowitz and I. A. Stegun, Eds. Washington, DC, USA: U.S. Government Printing Office, Dec. 1972.
[40] L. Isserlis, "On a formula for the product-moment coefficient of any order of a normal frequency distribution in any number of variables," *Biometrika*, vol. 12, nos. 1–2, pp. 134–139, 1918, doi: 10.1093/BIOMET/12.1-2.134.
[41] I. R. Savage, "Probability inequalities of the Tchebycheff type," *J. Res. Nat. Bur. Standards-B. Math. Math. Phys. B*, vol. 65B, no. 3, pp. 211–222, 1961.
[42] Y. T. Lo, "A probabilistic approach to the problem of large antenna arrays," *Radio Sci.*, vol. 68D, pp. 1011–1019, Sep. 1964.
[43] B. D. Steinberg, *Principles of Aperture & Array System Design*. New York, NY, USA: Wiley, 1976.
[44] A. Nuttall, "Some integrals involving the Q_M function (corresp.)," *IEEE Trans. Inf. Theory*, vol. IT-21, no. 1, pp. 95–96, Jan. 1975.
[45] R. Hansen, "A one-parameter circular aperture distribution with narrow beamwidth and low sidelobes," *IEEE Trans. Antennas Propag.*, vol. AP-24, no. 4, pp. 477–480, Jul. 1976.

Giovanni Buonanno (Member, IEEE) received the M.S. degree (summa cum laude) in electronic engineering from the Seconda Università degli Studi di Napoli (SUN), Aversa, Italy, in 2014, and the Ph.D. degree in industrial and information engineering from the University of Campania "Luigi Vanvitelli," Caserta, Italy, in 2018.

After his M.S. degree, he joined the research group in applied electromagnetics, SUN. He is currently a Research Fellow with the University of Calabria, Arcavacata, Italy. His research interests include the analysis and design of nonuniformly spaced antenna arrays, biomedical applications, and signal processing.

Sandra Costanzo (Senior Member, IEEE) received the Laurea degree (summa cum laude) in computer engineering from the Università della Calabria, Rende, Italy, in 1996, and the Ph.D. degree in electronic engineering from the Università Mediterranea di Reggio Calabria, Reggio Calabria, Italy, in 2000.

In 2017, she awarded the Italian National Scientific Qualification for the Full Professor position. Since 2019, she has been an Associate with IREA-CNR, Naples, Italy. She is currently an Associate Professor with the Università della Calabria, where she is the Coordinator of master's degree in telecommunication engineering and the Rector's Delegate for Security, Protection and Control of Electromagnetic Fields. She teaches courses on electromagnetic wave propagation, antennas, remote sensing, radar, sensors, and electromagnetic diagnostics. She is an Editor of the books *Microwave Materials Characterization* (INTECH, 2012) and *Wave Propagation Concepts for Near-Future Telecommunication Systems* (INTECH, 2017). She has authored or coauthored over 200 contributions in international journals, books, and conferences. Her research interests are focused on near-/far-field techniques, antenna measurement techniques, antenna analysis and synthesis, numerical methods in electromagnetics, millimeter-wave antennas, reflectarrays, synthesis methods for microwave structures, electromagnetic characterization of materials, biomedical applications, and radar technologies.

Dr. Costanzo is a member of the IEEE MTT-28 Biological Effects and Medical Applications Committee, the IEEE South Italy Geoscience and Remote Sensing Chapter, the Consorzio Nazionale Interuniversitario per le Telecomunicazioni (CNIT), the Società Italiana di Elettromagnetismo (SIEM), and the Centro Interuniversitario sulle Interazioni fra Campi Elettromagnetici e Biosistemi (ICEMB), and a Board Member of the IEEE AP/ED/MTT North Italy Chapter. She received the Telecom Prize for the Best Laurea Thesis in 1996 and the Best Academia and Research Application in Aerospace and Defense 2013 Award for the application software-defined radar using the NI USRP 2920 platform. She is an Associate Editor of IEEE ACCESS, IEEE JOURNAL OF ELECTROMAGNETICS, RF AND MICROWAVES IN MEDICINE AND BIOLOGY, and *Electronics* (section "Microwave and Wireless Communications") and an Editorial Board Member of *Radioengineering* and *International Journal of RF and Microwave Computer-Aided Engineering*. She was a Lead Editor of Special Issues titled: Reflectarray Antennas: Analysis and Synthesis Techniques in 2012, Advances in Radar Technologies in 2013, Compressed Sensing: Applications in Radar and Communications in 2016, Bioengineering Applications of Electromagnetic Wave Propagation in 2019, and Microwave Sensors for Biomedical Applications in 2020.

Raffaele Solimene (Senior Member, IEEE) received the Laurea (summa cum laude) and Ph.D. degrees in electronic engineering from the Seconda Università degli Studi di Naples (SUN), Aversa, Italy, in 1999 and 2003, respectively.

In 2002, he became an Assistant Professor at the Faculty of Engineering, Mediterranea University of Reggio Calabria, Reggio Calabria, Italy. Since 2006, he has been with the Dipartimento di Ingegneria, University of Campania "Luigi Vanvitelli," Caserta, Italy, where he is currently an Associate Professor. He holds an adjoint position at IIT Madras, Chennai, India. In 2017, he awarded the Italian National Scientific Qualification for the Full Professor position. His research interests include inverse electromagnetic problems with applications to inverse source and inverse scattering, nondestructive subsurface investigations, through-the-wall and GPR imaging, microwave medical imaging, array diagnostics, and random arrays. On these topics, he has authored or coauthored more than 250 scientific works, routinely serves as a reviewer for a number of journals, and organized several scientific sessions.

Dr. Solimene is a member of the Società Italiana di Elettromagnetismo (SIEM), the Consorzio Nazionale Interuniversitario per le Telecomunicazioni (CNIT), and Centro Interuniversitario sulle Interazioni fra Campi Elettromagnetici e Biosistemi (ICEMB). He is an Associate Editor of IEEE GEOSCIENCE AND REMOTE SENSING LETTERS, *Mathematical Problems in Engineering*, and *International Journal of Antennas and Propagation and Electronics* (section "Microwave and Wireless Communications").

Open Access funding provided by 'Università della Calabria' within the CRUI CARE Agreement